Transactions of the Korean Nuclear Society Spring Meeting
Jeju, Korea, May 8-10, 2024

A Study on Application of Sliding Mode Observer for Enhanced Load-Follow Operation in PWR

Husam Khalefih, andYonghee Kim
Department of Nuclear and Quantum Engineering, Korea Advanced Institute of Science and Technology (KAIST)
291 Daehak-ro, Yuseong-gu, Daejeon, 34141, Republic of Korea
husam.khalefih@kaist.ac.kr, yongheekim@kaist.ac.kr

***Keywords**: Load-Follow Operation, APR1400, Sliding Mode Observer, Xenon*

1. Introduction

Load Follow Operation (LFO) represents a significant advancement in the operation of Pressurized Water Reactors (PWRs). It involves adjusting the reactor's thermal power output to match changes in electricity demand, either daily or seasonally [1]. However, this process entails complex steps and procedures to ensure adherence to reactor safety parameters at all times. One critical parameter that must be managed is the boron concentration in the reactor core. Generally, plant operators manually adjust the boron concentration to compensate for fuel burnup (BU) during base load operation. Nevertheless, during LFO, numerous reactivity feedbacks occur that cannot be managed solely through Control Element Assemblies (CEA). As a result, the soluble boron concentration in the reactor core must be carefully adjusted, especially during rapid and significant power ramp-up/down phases [2,3].

Adjusting boron concentration in the reactor core is usually done to offset changes in xenon concentration. In large-size PWRs, the equilibrium xenon worth can reach up to 3500 pcm. Accurately estimating the required boron concentration during LFO necessitates an understanding of the changes in xenon concentration in the reactor core. Since xenon concentration is not directly measurable online within the reactor core, researchers have explored various methods to predict or observe it. Dr. Utikin was the first to propose using the Sliding Mode Observer (SMO) to monitor various unmeasurable quantities in the reactor core, such as reactivity and delayed neutron precursors [4]. Similarly, Dr. Ansafari applied the SMO to estimate the xenon stability index in the reactor core, employing a multipoint, point reactor kinetic model [5]. Other studies have aimed to estimate xenon concentration or temperature changes in different reactors, such as High-Temperature Gas-Cooled Reactors (HTGR) [6].

This study introduces the use of the SMO to estimate xenon concentration during LFO in the APR1400. It will also present a detailed strategy for using this information to determine the necessary adjustments in boron concentration. The analysis was performed using the in-house reactor simulator code KANT, a NEM-CMFD accelerated diffusion code, with two-group cross-sections generated by the SERPENT 2 Monte Carlo code and validated using the ENDF/B-VII data library. [7,8].

2. Reactor Description

The analysis was performed on the erbium-based LEU+ loaded APR1400 reactor core design [9]. In this design, a two-batch APR1400 core configuration was achieved by utilizing erbium and gadolinium as burnable absorbers and fuel assemblies with an enrichment higher than 5.0 w/o. Figure 1 illustrates the core loading pattern and the design of the fuel assemblies [10].

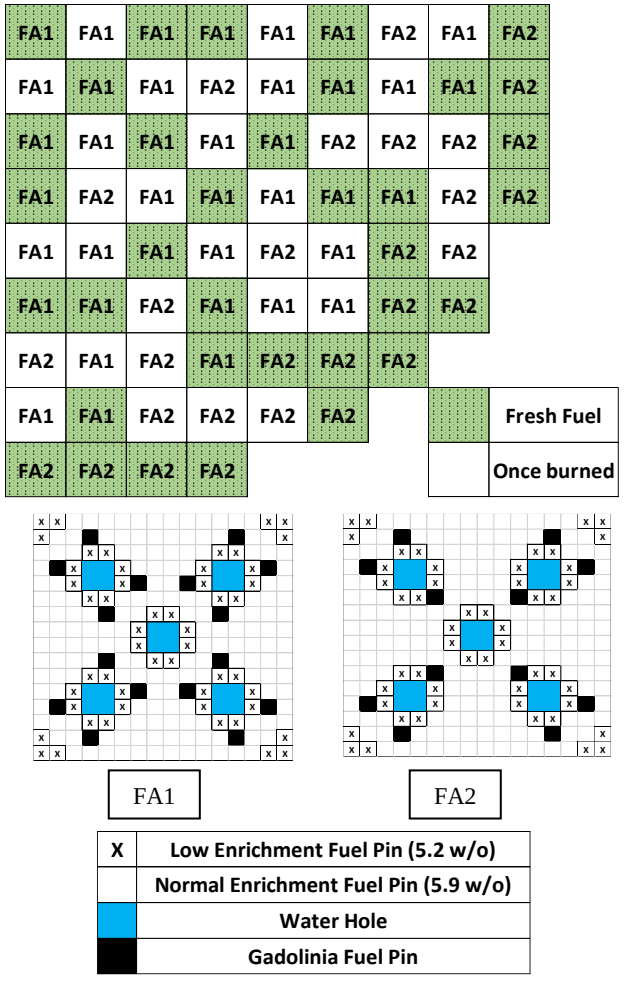

Figure 1 Er and LEU+ base two batches APR1400 fuel loading pattern and design.

3. Sliding Mode Observer Model

Eq. (1)-(3) show the general definition of the sliding mode observer, where x, and $\hat{x}$ represent the actual and observable system states, respectively. The function f governs the changes in system parameters, and $\dot{e}$ is the dynamic error between the actual parameter value and the observable one.

$$\dot{x} = f(x,u) + g(x,u) \quad (1)$$
$$\dot{\hat{x}} = f(\hat{x},u) + L(\hat{x} - x) \quad (2)$$
$$\dot{e} = \dot{\hat{x}} - \dot{x} \quad (3)$$

Eq. (4)-(12) describes the SMO system of equations, which are based on the point reactor model. It is crucial to determine the values of the gains (k, ψ), which determine the stability of the solution as well as the speed of convergence to the sliding surface. The selection of these parameters should be based on Lyapunov stability analysis, where the Lyapunov function is defined by the half-square of all errors and the resulting function derivative should be negative definite to ensure reaching a local stable minimum.

$$\dot{\hat{p}} = \frac{\hat{\rho} - \beta}{\Lambda}\hat{p} + \sum_{i=1}^{6}\lambda_i\hat{C}_i + \boldsymbol{k_1}(p - \hat{p}) + \boldsymbol{\psi_1}\tanh\left(\frac{p-\hat{p}}{\varphi}\right) \quad (4)$$

$$\dot{\hat{C}}_i = \frac{\beta_i}{\Lambda}p - \lambda_i\hat{C}_i + \boldsymbol{k_{i+1}}(p - \hat{p}) + \boldsymbol{\psi_{i+1}}\tanh\left(\frac{p-\hat{p}}{\varphi}\right) \quad (5)$$

$$M_f c_f \frac{dT_f}{dt} = \hat{p}(t)p_0 - \frac{1}{R_g}\left[T_f(t) - T_{cl}(t)\right] \quad (6)$$

$$M_{cl}c_{cl}\frac{dT_{cl}}{dt} = \frac{1}{R_g}\left[T_f(t) - T_{cl}(t)\right] - \frac{1}{R_c}\left[T_{cl}(t) - T_c(t)\right] \quad (7)$$

$$M_c c_c \frac{dT_c}{dt} = \frac{1}{R_c}[T_{cl}(t) - T_c(t)] - 2w(t)c_c[T_c(t) - T_i(t)] \quad (8)$$

$$\dot{\hat{I}} = \gamma_I\Sigma_f\hat{\phi} - \lambda_I\hat{I} + \boldsymbol{k_8}(p - \hat{p}) + \boldsymbol{\psi_8}\tanh\left(\frac{p-\hat{p}}{\varphi}\right) \quad (9)$$

$$\dot{\hat{X}} = \gamma_X\Sigma_f\hat{\phi} + \lambda_I\hat{I} - \lambda_X\hat{X} - \sigma_X\hat{X}\hat{\phi} + \boldsymbol{k_9}(p - \hat{p}) + \boldsymbol{\psi_9}\tanh\left(\frac{p-\hat{p}}{\varphi}\right) \quad (10)$$

$$\hat{\rho} = \rho_r + \alpha_f\left(T_f - T_{f0}\right) + \alpha_c(T_c - T_{c0}) - \frac{\sigma_a^{Xe}(\hat{X} - \hat{X}_0)}{\Sigma_f} \quad (11)$$

$$\dot{\rho}_r = G_r Z_r \quad (12)$$

where p is the normalized reactor power, $\hat{\rho}$ is the observed reactivity, C_i, λ_i, and β_i are the group i delayed neutron precursor concentration, decay constant, and delayed neutron fraction. M_f, M_{cl}, and M_c are the fuel, clad, and coolant mass (kg). T_f, T_{cl}, and T_c are the fuel, clad, and coolant temperatures. R_c, and R_g are the thermal resistance between the coolant-clad, and fuel-clad, respectively. $\hat{I}$, $\hat{X}$ are the iodine-135 and xenon-135 concentration (#/cm^3), α_f, α_c are the fuel and coolant reactivity coefficients (pcm/C), ρ_r, G_r, Z_r are the control rod reactivity, worth, and moving speed respectively.

The speed of control rod movement to achieve the required reactivity change during LFO should be determined using an adaptive control strategy. Eq. (13) shows the system input value, which is the control rod speed.

$$Z_r = \frac{\Lambda}{nG_r}\left[\ddot{n}_d - m\dot{e} - \eta\tanh\left(\frac{s}{\varphi}\right) - \frac{\hat{\rho} - \beta}{\Lambda}\dot{n} - \sum_{i=1}^{6}\lambda_i\hat{C}_i\right] - \frac{1}{G_r}\left[\alpha_f\dot{T}_f + \alpha_c\dot{T}_c - \frac{\sigma_a^{Xe}\hat{X}}{\Sigma_f}\right] \quad (13)$$

In this analysis, the system power p, is the only measurable quantity during reactor operation, which is obtained from the reactor regulating system. The deviation of this power from the observable power $\hat{p}$ is determined to initiate the movement of system trajectories toward the sliding surface.

Table 1 shows the value of the parameters used in this analysis. Notice that in this analysis, the most important parameters are the macroscopic fission cross-section and the xenon microscopic absorption cross-section which are necessary to determine the xenon and flux values in the reactor core.

Table 1 The SMO parameters values.

Parameter	Value
c_f (J/kg.K)	247
c_{cl} (J/kg.K)	330
c_c (J/kg.K)	6748
M_f (kg)	65722
M_{cl} (kg)	13539
M_c (kg)	151456
w (kg/sec)	10516
α_f (Δk/k/°C)	-3.24E-05
α_c (Δk/k/°C)	-2.13E-04

G_r (pcm)	14.5E-3

4. Computational Tool

Figure 2 showcases the flow diagram for the KANT simulation modules. The initial conditions, power profile, and temperatures are first initiated by KANT through the steady-state modules. Following this, the standard KANT models are invoked to start the time-dependent simulation of the reactor core. This involves solving the time-dependent diffusion equation and the transient thermal-hydraulic modules. From this, the reactor power (p) is provided to the SMO module to solve the system of equations described in Section 3. Since the initial condition of the xenon concentration is arbitrarily determined, the LFO will not be initiated until the equilibrium xenon concentration is achieved [11].

After determining the on-the-fly xenon concentration and using the conversion factors, the required boron concentration adjustment will be determined. To accomplish this, the equilibrium xenon concentration using the SMO shall be determined, and boron worth (pcm/ppm) and the equilibrium xenon worth (pcm) shall also be provided. Usually, these quantities can be accurately measured or calculated before the initiation of the BU cycle and are provided via the technical specifications.

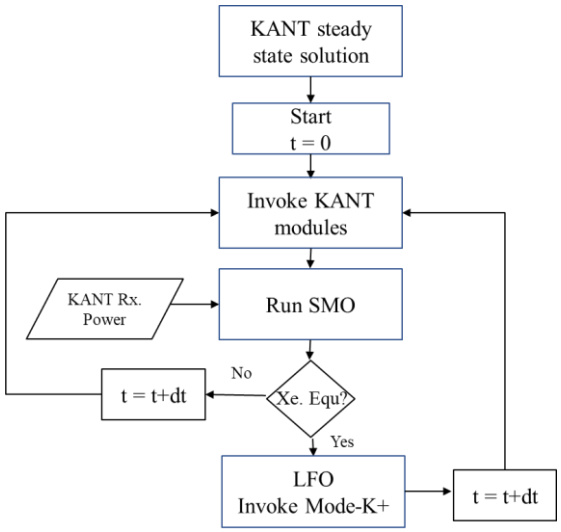

Figure 2 KANT simulation flow diagram.

5. Results and Discussion

To assess the performance of the SMO, simulations at the Mid of Cycle (MOC) and End of Cycle (EOC) of the Er-based APR1400 equilibrium core were conducted. Figure 3 depicts a 120-hour LFO using KANT and SMO-assessed simulation. It was found that the observed reactor power successfully follows the reactor power (KANT power), taking approximately 40 hours to reach the equilibrium xenon concentration before the LFO scenario begins. Meanwhile, the observed xenon concentration shows a very good match with the transient xenon calculated via the 3D KANT simulations, with an error of less than 2% during the LFO, following the achievement of xenon equilibrium.

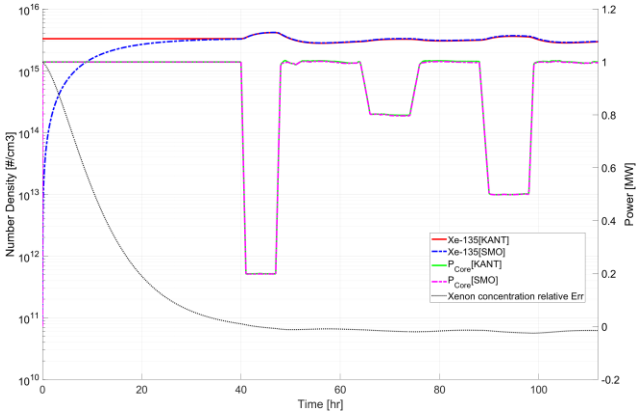

Figure 3 LFO at the MOC condition using KANT and SMO assessed simulation.

A similar analysis was also conducted at the EOC BU condition, which has a much higher BU value. Figure 4 showcases a similar strategy at the EOC, with 96 hours of daily LFO scenarios. It was also observed that the SMO observed xenon concentration matches very well with the reference 3D KANT calculated core xenon concentration. This indicates that the SMO works very well with realistic system simulations, maintaining an acceptable error margin. Note that the exact xenon concentration in the reactor core is not necessary since the important factor here is to determine the behavior and rate of xenon concentration change in the reactor core.

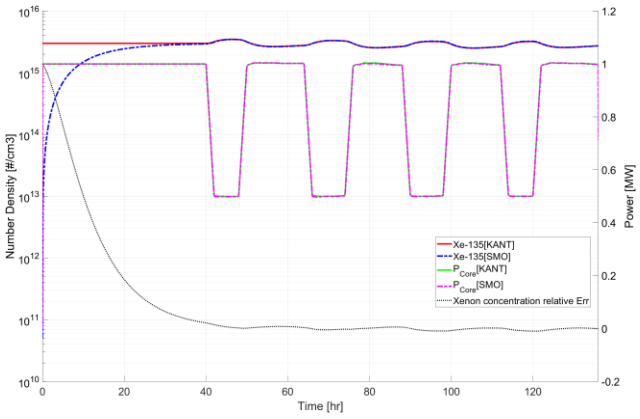

Figure 4 LFO at the EOC with a comparison between KANT 3D calculated xenon concentration and the SMO observed value.

It is worth mentioning that the detailed LFO performed in the KANT 3D model is based on the mode-K+ control algorithm. This assumes that the soluble boron scenario is

manually selected by the operator after trial and error, and based on their experience. A more systematic approach, based on the information on the xenon concentration change, should be adopted for more reliable control.

6. Conclusions and Future Work

Improving the economic impact of nuclear power plants requires enhancing the capability to perform Load Following Operations (LFO). One of the most important parameters to be determined during the LFO is the adjustment of boron concentration. The boron dilution/boration process should be carried out to compensate for changes in xenon concentration in the reactor core during the LFO. Hence, prior knowledge of the unmeasurable xenon concentration in the reactor core would provide valuable information for reactor operators regarding the required actions.

A Sliding Mode Observer (SMO) was designed to monitor the xenon concentration in the core, where the only measurable quantity, the reactor power, is provided to the SMO module via the KANT-calculated reactor power. Then, using Lyapunov stability analysis, the gain values needed to determine the stability of the observer are determined. The performance of the observer was analyzed by performing LFOs in the Er-based APR1400 equilibrium cycle at different burnup (BU) levels, and the results show a very good agreement between the observed xenon concentration and the one calculated using KANT 3D.

For future work, a detailed strategy for utilizing information on xenon concentration to determine the necessary boron adjustment scenario will be discussed. Additionally, the impact of the uncertainty of calculation parameters, such as the macroscopic fission and microscopic xenon absorption cross-sections on the xenon estimation, will be investigated.

ACKNOWLEDGMENT

This work was supported by the National Research Foundation of Korea (NRF) Grant funded by the Korean Government (MSIT) (RS-2022-00144429, and 2022M2E9A304619011).

REFERENCES

[1] Lokhov, A., 2011. Technical and economic aspects of load following with nuclear power plants. NEA, OECD, Paris, France, 2.
[2] Khalefih, Husam, Yunseok Jeong, and Yonghee Kim. "Daily Load-Follow Operation in LEU+-Loaded APR1400 Using Mode-K+ Control Logic." International Journal of Energy Research 2023 (2023).
[3] Khalefih, Husam, and Yonghee Kim. "A Study on Control Algorithm for Daily Load-Follow Operation in the APR1400 Reactor." In American Nuclear Society Winter Meeting, vol. 127, pp. 1145-1148. 2022.
[4] Wang, P., Aldemir, T. and Utkin, V.I., 2001, December. Estimation of xenon concentration and reactivity in nuclear reactors using sliding mode observers. In Proceedings of the 40th IEEE Conference on Decision and Control (Cat. No. 01CH37228) (Vol. 2, pp. 1801-1806). IEEE.
[5] G.R. Ansarifar, M.H. Esteki, M. Arghand, Sliding mode observer design for a PWR to estimate the xenon concentration & delayed neutrons precursor density based on the two point nuclear reactor model, Progress in Nuclear Energy, Volume 79, 2015, Pages 104-114, ISSN 0149-1970.
[6] Žerovnik, G., Čalič, D., Gerkšič, S., Kromar, M., Malec, J., Mihelčič, A., Trkov, A. and Snoj, L., 2023. An overview of power reactor kinetics and control in load-following operation modes. Frontiers in Energy Research, 11, p.1111357
[7] Taesuk Oh, Yunseok Jeong, Husam Khalefih, Yonghee Kim, Development and validation of multiphysics PWR core simulator KANT, Nuclear Engineering and Technology, Volume 55, Issue 6,2023, Pages 2230-2245, ISSN 1738-5733.
[8] Leppänen, J., Pusa, M., Viitanen, T., Valtavirta, V. and Kaltiaisenaho, T., 2015. The Serpent Monte Carlo code: Status, development and applications in 2013. Annals of Nuclear Energy, 82, pp.142-150.
[9] U.S. Nuclear Regulatory Commission. "AP1000 Design Control Document: Chapter 4, Tier 2." Revision 19. PDF file: https://www.nrc.gov/docs/ML1117/ML11171A445.pdf.
[10] 13. Khalefih, H., Oh, T., Jeong, Y. and Kim, Y., 2023. LEU+ loaded APR1400 using accident-tolerant fuel cladding for 24-month two-batch fuel management scheme. Nuclear Engineering and Technology, 55(7), pp.2578-2590.
[11] Khalefih, H., Jeong, Y. and Kim, Y., “A Study on Daily Load-follow Operation in the APR1400 Reactor using Manganese-Based Partial Strength Control Element Assembly,” *Proc. Korea Nuclear Society*, Korea, Oct. 2022.